Dyes and Pigments 191 (2021) 109373

Contents lists available at ScienceDirect

Dyes and Pigments

journal homepage: http://www.elsevier.com/locate/dyepig

A novel reactive chemosensor for sulfide detection with high selectivity and sensitivity based on 4-Cl coumarin derivatives

Hongda Li [a,*], Yunfan Yang [b,**], Xiaojing Wu [c], Rulin Jia [a], Pengcheng Zhao [a], Yan Wang [a]

[a] Department of Forensic Chemistry, Criminal Investigation Police University of China, Shenyang, 110035, China
[b] Key Laboratory for Microstructural Material Physics of Hebei Province, School of Science, Yanshan University, Qinhuangdao, 066004, China
[c] Institute of Functional Molecules, Shenyang University of Chemical Technology, Shenyang, 110142, China

ARTICLE INFO

Keywords:
Sulfide detection
4-Cl Coumarin
Substitution reaction
Quantum chemistry calculation
Water samples

ABSTRACT

We describe the design and synthesis of a novel reactive chemosensor based on 4-Cl Coumarin derivatives. This chemosensor displays significantly fluorescence performance in the detection of sulfur ions in water samples, and the inactive mechanism has been clearly demonstrated via fluorescence titration, Job's plot, ESI-MS, ^{1}H NMR and Quantum chemistry calculation.

1. Introduction

Sulfide (sodium sulfide, barium sulfide, hydrogen sulfide, etc.) exists naturally, but also as a by-product of medicine synthesis, industrial production, and military industry [1]. Large concentrations of sulfide compounds in the water or air can be toxic to both the natural environment and human health, and can potentially pose great risk. People smoking too much sulfide can lead to diseases such as diabetes, high blood pressure, liver cirrhosis, down syndrome [2]. In China, sulfur content is one of the commonly used indices of drinking water quality. Regulations stipulate that the groundwater sulfide concentration must not exceed 1 mg/L, and sulfide concentration in drinking water shall not be more than 0.02 mg/L (GB5749-2006). At present, there are many kinds of test methods for the different sulfur ions, and each have shortcomings. The principle detection methods include; iodine quantity method, inductively coupled plasma atomic emission spectroscopy, hydride generation atomic fluorescence spectrometry, electrochemical methods, ion chromatography, spectrophotometry, fluorimetry, and chemosensory methods. These analysis methods typically have low sensitivity, large sample demands, complicated pretreatment protocols, or are otherwise time-consuming. Therefore, the development of a simple, fast method with a high sensitivity, good selectivity has important practical significance (see Scheme 1).

The chemosensor has gained wide attention in environmental monitoring and biology [3–13]. Reactive chemosensors the combination of the analyte was generally through the irreversible chemical reaction. The sulfide reactive chemosensor, based on the nucleophilic character of sulfides, had the advantages of rapid response and high sensitivity and selectivity. Recently, the superior performance of sulfide reactive chemosensors have been reported [7,14–16]. These chemosensors mainly identified the presence of sulfide via an azide reduction reaction [17,18], nitro reduction reaction [13,19], double bond addition reaction [20,21], cleavage reaction of the R–O or R–S bond [22,23].

In this paper, we report a sulfide reactive chemosensor based on 4-Cl coumarin derivatives. Coumarin derivatives were used as chromophores because of their excellent optical properties. In aromatic halogen molecules, the C-X bond forms a polar covalent bond, with a partial positive charge of carbon atoms susceptible to attack of a nucleophilic reagent (: Nu-) in the form of a substitution of the halogen atom to form a new C-Nu bond, which can cause the optical signal of the chemosensor to change. This can provide a quantitative, accurate sulfide identification method.

2. Experimental section

2.1. Materials and instruments

All of the raw materials were sourced from J&K Scientific Ltd. Sodium sulfide and other analysts were sourced from Sinopharm Chemical Reagent Shenyang co. Lid. All of the organic solvents, such as methanol,

* Corresponding author.,
** Corresponding author.
E-mail addresses: lihongda@cipuc.edu.cn, lhd870821@163.com (H. Li), yangyunfan2626@163.com (Y. Yang).

https://doi.org/10.1016/j.dyepig.2021.109373
Received 12 January 2021; Received in revised form 27 March 2021; Accepted 3 April 2021
Available online 16 April 2021

ethanol, ethyl acetate, methylene chloride, dimethyl sulfoxide (DMSO) were sourced from Sinopharm Chemical Reagent Shenyang co. Lid. And which had not been purified to use directly.

The structure characterized were measured by the Bruker AV-300 Spetrometer (300 MHz for ^{1}H NMR) and the Thermo Scientific Orbitrap Exploris 480 spectrometer (HRMS).

2.2. Synthesis and characterization of chemosensor 1

Chemosensor 1 was prepared by a simple Knoevenagel condensation reaction between 4-chloro-7-(diethylamino)-3-formyl-coumarin (2) and acetophenone. The 4-chloro-7-(diethylamino)-3-formyl-coumarin (2) was prepared according to the reported literature [24].

The compound 2 (1.9 g, 6.8 mmol) and acetophenone (2.0 g, 16.7 mmol) were dissolved in dry EtOH (5.0 mL). To the solution was added piperidine (3–4 drops) at 80 °C and stirred for 1.5 h. The resulting solid was filtrated and washed with cold diethyl ether. The residue was recrystallized from MeOH to obtain the desired product **1** as a yellow solid 1.063 g (55.8%).

^{1}H NMR (300 MHz , DMSO-d_6 , ppm) δ: 8.35–8.28 (1H, d, –CH_2═CH_2-, J = 15.2 Hz), 8.02–7.96 (3H, m, –CH═CH- and Ar–H), 7.76–7.72 (1H, d, J = 9.2 Hz, Ar–H), 7.71–7.64 (1H, m, Ar–H), 7.63–7.55 (3H, m, Ar–H), 6.92–6.86 (1H, dd, J_1 = 2.4 Hz, J_2 = 9.2 Hz, Ar–H), 6.67–6.33 (d, 1H, J = 2.4 Hz, Ar–H), 3.55–3.46 (4H, q, J = 7.0 Hz, -CH_2-CH_3), 1.19–1.11 (6H, t, J = 7.0 Hz, –CH_3-CH_3). ^{13}C NMR (75 MHz, DMSO-d_6. ppm) δ: 189.82, 158.56, 154.86, 153.00, 151.08, 138.27, 135.89, 133.58, 129.44, 128.56, 128.35, 124.48, 111.35, 111.20, 107.37, 96.53, 44.94, 12.84. HRMS *m/z*: $[M+H]^+$ at 382.1194. Calcd for $C_{22}H_{21}^{35}ClNO_3^+$ ($[M+H]^+$) 382.1132. $[M+H]^+$ at 384.1162. Calcd for $C_{22}H_{21}^{37}ClNO_3^+$ ($[M+H]^+$) 382.1102.

2.3. Synthesis and characterization of compound 1-S^{2-}

The solution of Na_2S (0.015 g, 0.2 mmol, in 2 mL of H_2O) was added to the solution **1** (0.05 g, 0.13 mmol, in 8 mL of CH_3CN). The mixture was stirred for 3 h at room temperature. Remove the solvent by vacuum, and 50 mL of water was added to the mixture and extracted with 200 mL of ethyl acetate for three times, dried over anhydrous Na_2SO_4. After the removal of solvent, the product was purified by silica gel column chromatography (ethyl acetate: petroleum ether, 1:10) to yield light yellow solid (28.7 mg, 58.2%).

^{1}H NMR (300 MHz , DMSO-d_6 , ppm) δ: 9.08–9.03(1H, d, J = 15.2 Hz, –CH_2═CH_2-), 8.35–8.32 (1H, d, J = 9.2 Hz, Ar–H), 8.17–8.12 (1H, d, J = 15.2 Hz, –CH═CH-), 7.92–7.89 (2H, dd, J_1 = 1.8 Hz, J_2 = 8.1 Hz, Ar–H), 7.58–7.50 (3H, m, Ar–H), 6.62–6.58 (1H, dd, J_1 = 1.8 Hz, J_2 = 9.0 Hz, Ar–H), 6.25–6.24 (d, 1H, J = 2.4 Hz, Ar–H), 3.45–3.37 (4H, q, J = 6.9 Hz, -CH_2-CH_3), 1.16–1.11 (6H, t, J = 6.9 Hz, –CH_3-CH_3). ^{13}C NMR (75 MHz, DMSO-d_6. ppm) δ: 191.84, 190.38, 160.19, 153.24, 150.90, 147.13, 140.08, 132.30, 132.06, 129.05, 128.13, 116.51, 115.58, 111.34, 108.69, 95.52, 44.47, 12.81. HRMS *m/z*: $[M+H]^+$ at 380.1305. Calcd for $C_{22}H_{22}NO_3S^+$ ($[M+H]^+$) 380.1242.

2.4. General optical measurements

Stock solution A of chemosensor 1 (0.5 mmol/L) was prepared in DMSO. Stock solutions B of various analytes (1 mmol/L for NaF, NaCl, NaBr, NaI, $KClO_3$, $KClO_4$, Na_2SO_4, $NaHSO_3$, KNO_3, $NaNO_2$, KH_2PO_4, CH_3COONa, NaN_3, L-Cys, Hcy, GSH) were prepared in PBS buffer solution (pH 7.4, 10 mmol/L). For optical measurements, Mix Stock solution A and Stock solutions B evenly in proportion to form test solutions. The excitation wavelength was set at 460 nm and the slit sizes were 5-5 nm, respectively.

2.5. Method for Quantum chemistry calculation

Theoretical calculations of compounds 1 and 1-S^{2-} in DMSO solvent were carried out with density functional theory (DFT) and time-dependent DFT (TDDFT). The surrounding solvent environment was stimulated by general solvation model of solute electron density (SMD) [25]. Static and dynamic dielectric constants (eps and epsinf) of the [DMSO: H_2O (8:2)] PBS buffer were 53.13186 and 2.09728, respectively. The geometric structures before and after detecting analytes were fully optimized by long-range hybrid exchange correlation functional ωB97XD [26] with basis set 6-31 + G (d, p). Their Infrared (IR) vibrational frequencies of different degrees of freedom were also calculated with the same method as optimization. In excited state, the geometric structures and their IR vibrational frequencies were optimized and calculated by the theoretical level of TD-ωB97XD/6-31 + G (d, p). The nonexistent vibrational imaginary frequencies indicated that the optimized geometric structures were optimal. In the photoexcitation process, we analyzed the redistribution of electron densities based on theoretical level of TD-ωB97XD/6-31 + G (d, p), and the frontier

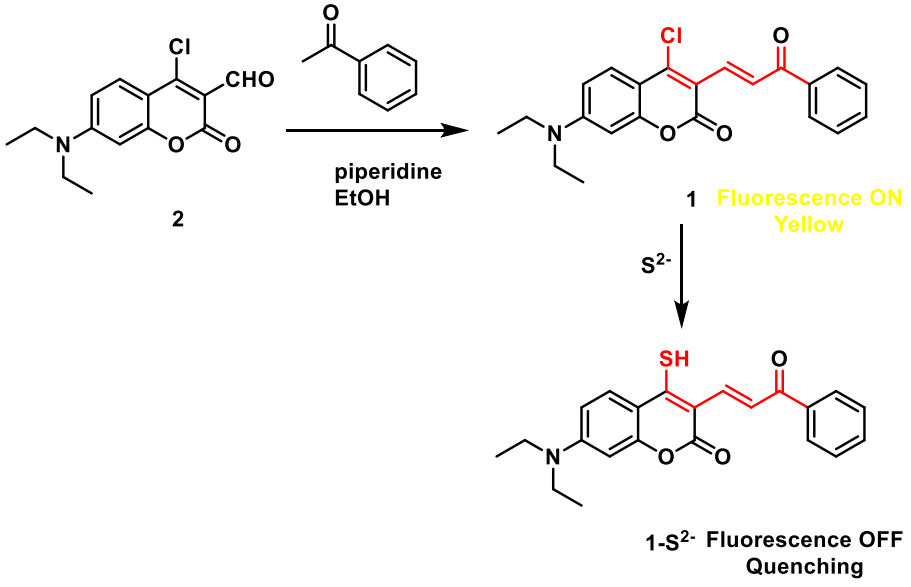

Scheme 1. Synthesis of chemosensor **1** and the sensor mechanism of chemosensor **1** for S^{2-}

molecular orbitals (FMOs) were drawn by Chemcraft program. In addition, excitation and emission energies were calculated by using the functional B3LYP [27] and basis set 6-31 + G (d, p). All electron spectra were fitted with Gauss view 5.0 visual suite. The whole theoretical calculations were performed by Gaussian 09 Revision D.01 program. Linearly interpolated internal coordinates (LIICs) of 1-S^{2-} were calculated follow the rotation of 4-sulfydryl group in different electronic states.

3. Results and discussion

3.1. The time-dependent of chemosensor 1 for S^{2-}

In order to evaluate its reactivity, time-dependent UV–vis spectra were collected of chemosensor **1** (10 μmol/L) in response to S^{2-} (50 μmol/L) in PBS buffer (pH 7.40, 10 mmol/L, contains 80% DMSO) solution. As shown in Fig. 1, chemosensor **1** exhibited a main peak at 480 nm, characteristic of the coumarin and α, β-unsaturated ketone moiety. Upon treatment with S^{2-}, the absorption peak at 480 nm decreased gradually, coupled with the appearance of two new peaks at 415 and 458 nm. The peak at 458 nm can be attributed to the C-SH group in the reaction product, and reached a maximum after about 10 min. The calculated pseudo-first-order rate constant (k') was 0.414 ± 0.009 min^{-1} (Fig. 1 inset). This observation suggested that chemosensor **1** can identify S^{2-} rapidly in PBS buffer (pH 7.40, 10 mmol/L, contains 80% DMSO) solution.

3.2. The response of chemosensor 1 toward various analytes

The selectivity of chemosensor is one of the important factors impacting on the real-world sensing performance. Therefore, we studied the selectivity of chemosensor 1 to sulfur ions in PBS buffer (pH 7.40, 10 mmol/L, contains 80% DMSO) solution (Figs. 2, S1 and S2). The competitive analytes included: F^-, Cl^-, Br^-, I^-, ClO_3^-, ClO_4^-, SO_4^{2-}, HSO_3^-, NO_3^-, NO_2^-, $H_2PO_4^-$, CH_3COO^-, N_3^-, L-Cys, Hcy, GSH. The test results were shown in Fig. 2 and S1; chemosensor **1** shows a very strong fluorescence signal at 557 nm. Upon the addition of competitive analytes there is no significant change in fluorescence intensity of chemosensor **1** at 557 nm. Under the PBS buffer (pH 7.40, 10 mmol/L, contains 80% DMSO) solution, the chemosensor 1 for GSH, Cys, Hcy, SO_4^{2-} or HSO_3^- were not occurring Michael type additions (Fig. S2). It is only when sulfur ions are introduced that obvious fluorescence quenching is observed. Competition experiments were also conducted as shown in Fig. 2. When S^{2-} coexisted with other analytes, the fluorescence intensity of chemosensor **1** was still completely quenched. These results show that the chemosensor **1** is highly selective to S^{2-}, and the presence of other analytes does not provide impactful interference.

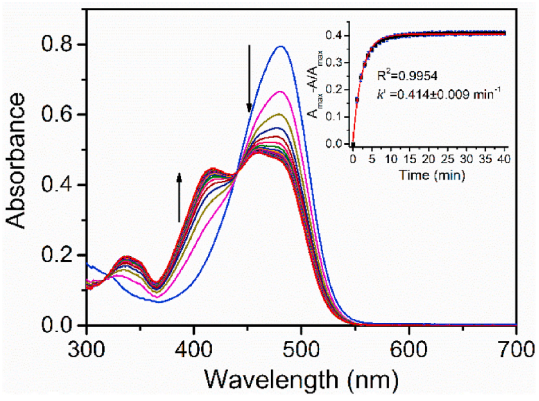

Fig. 1. The time-dependent UV–vis spectra of chemosensor 1 (10 μmol/L) to S^{2-} (50 μmol/L). Inset: The pseudo-first-order conditions.

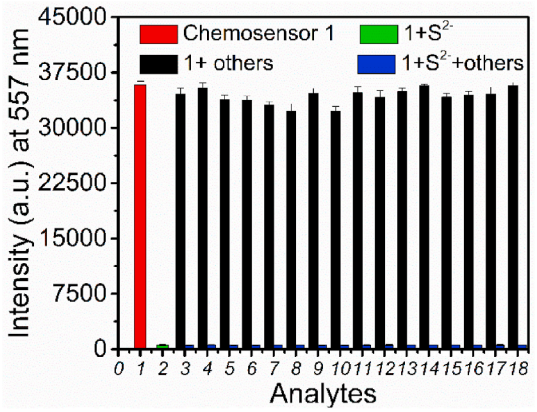

Fig. 2. Fluorescence intensities ($\lambda_{ex}/\lambda_{em}$ = 460/557 nm) of chemosensor 1 (10 μmol/L) in the presence or non-presence of 50 μmol/L for various analytes (Other analytes for F^-, Cl^-, Br^-, I^-, ClO_3^-, ClO_4^-, SO_4^{2-}, HSO_3^-, NO_3^-, NO_2^-, $H_2PO_4^-$, CH_3COO^-, N_3^-, L-Cys, Hcy, GSH).

3.3. The fluorescence response of chemosensor 1 toward S^{2-}

The sulfide fluorescence titration characteristics of chemosensor **1** were studied in PBS buffer (pH 7.40, 10 mmol/L, contains 80% DMSO) solution (Fig. 3). Upon addition of various concentrations of S^{2-} (from 0 μmol/L to 50 μmol/L), the fluorescence intensity at 557 nm decreased, with the quenching degree reaching 96.8% for 12 μmol/L of S^{2-} (Fig. 3). Meanwhile, the fluorescence intensity change of chemosensor **1** for various concentrations of S^{2-} (from 0 μmol/L to 10 μmol/L) shows a linear correlation (R^2 = 0.9997), with a calculated detection limit of 0.12 μmol/L (Fig. 3 inset).

3.4. Mechanism of the sensing of S^{2-}

In order to study the stoichiometric relationship between chemosensor **1** and S^{2-}, the Job's plot, ESI-MS, ^1H NMR and HPLC of substituted products were examined. The maximum value of Job's plot was 0.5 molecular fraction (Fig. S3), which suggests that the stoichiometric relationship was 1:1 between the chemosensor and S^{2-}. The ESI-MS spectrum of the chemosensor **1**-S^{2-} complex was studied in DMSO solution (Figs. S4 and S5). The signal at 378.20 (m/z) was assigned to the species [**1**-Cl^- + SH^- + H^+]$^+$, which further corroborates the 1:1 stoichiometric relationship. The sensing mechanism of chemosensor **1** for sulfur ion was studied by HPLC. The HPLC chromatogram of the chemosensor **1** and its substitution products (chemosensor **1** for Na_2S) were

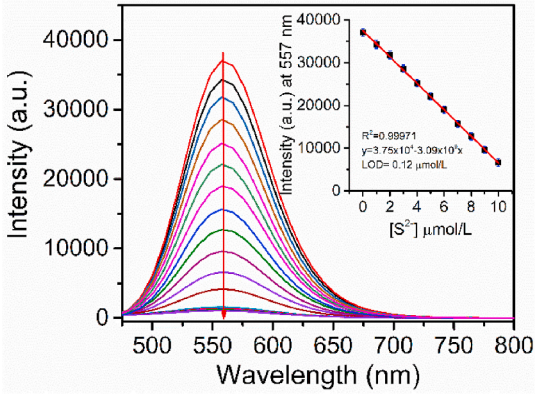

Fig. 3. Fluorescence spectra ($\lambda_{ex}/\lambda_{em}$ = 460/557 nm) of chemosensor 1 (10 μmol/L) with S^{2-}; Inset: The plot of fluorescence intensity difference with 1 (10 μmol/L) and S^{2-} from 0 to 10 μmol/L in PBS buffer (pH 7.40, 10 mmol/L, contains 80% DMSO) solution.

given in Figs. S6 and S7. The retention times of the identified peaks were obviously different in the absence (Fig. S6, t_R = 3.50 min) and presence (Fig. S7, t_R = 2.60 min) of Na_2S. The ^1H NMR of substituted products also supports the proposed sensing mechanism: as shown in Fig. 4, the proton signal 8.32 ppm (H_1) and 7.99 ppm (H_2) can be attributed to a *trans*-conjugated double bond in chemosensor **1**. Upon the addition of Na_2S at 1 equiv., the proton signal H_1 and H_2 were upfield shifted from 8.32 ppm to 9.05 ppm–7.99 ppm to 8.15, respectively. In addition, the number of proton signal Ar–H were not changed in the presence and absence of Na_2S. In addition, the fluorescence pH titrations were performed in buffer solution at a compound 1-S^{2-} concentration of 10 μmol/L. The pH-dependent fluorescence spectra were presented in Fig. S8. The results of the nonlinear regression at 557 nm according to a literature method [28], affording a pKa value of ~8.64. the compound 1-S^{2-} having the SH group had been confirmed as the dominating species in PBS buffer. Here, the ^1H NMR and pH-dependent fluorescence spectra further confirmed the predicted sensing mechanism as a substitution reaction at the C–Cl bond to form C-SH in PBS buffer (pH 7.40, 10 mmol/L, contains 80% DMSO) solution.

3.5. Quantum chemistry calculation

The configurations of Chemosensor 1 and product 1-S^{2-} were fully optimized with ωB97XD/6-31 + G (d, p) theoretical level in Fig. 5. We used the same level of theory as optimization to calculate molecular infrared vibrational frequencies, free from imaginary vibrational frequencies indicated that the structures optimized by our theoretical method were locally the most stable. In Fig. 5, we used the ball & bond model in intriguing portion, for the rest portion of structures, we used the tube model to display. For Chemosensor 1, the dihedral δ (OCCC) increased from 160.2° of ground (S_0) state to 160.5° of the first excited (S_1) state upon photoexcitation process. It was found that the rotation of benzene ring was nearly negligible, relative to coumarin portion. For 1-S^{2-} form, however the dihedral δ (OCCC) increased from 160.3° of S_0 state to 162.6° of S_1 state upon photoexcitation process. Note that after the C–Cl group of the product 1-S^{2-} molecule was replaced by C-SH, the sulfydryl group was more easier to generate out-of-plane rotation due to the stronger dipole interaction. The diheral δ (CCSH) was 20.4° in S_0 state, which enlarged to 30.9° in S_1 state. It indicated that C-SH might be more easier to form intermolecular hydrogen bonding interaction in S_1 state, induced the quenched of 1-S^{2-}.

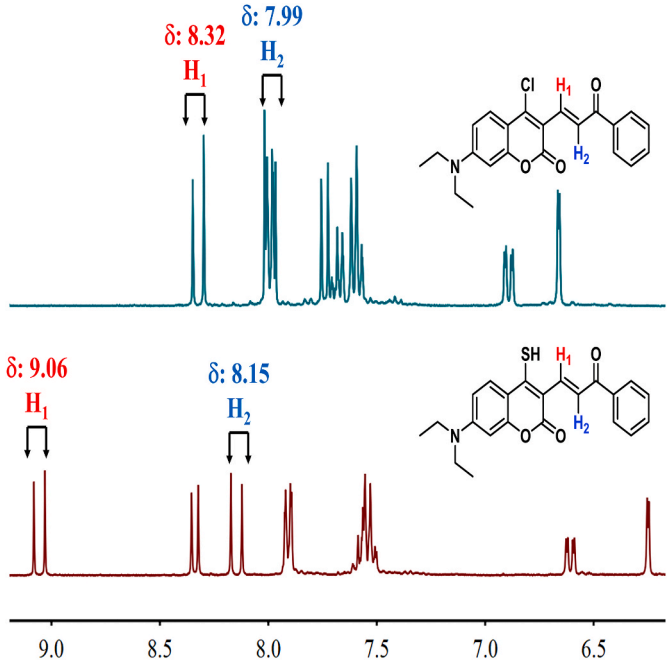

Fig. 4. Partial ^1H NMR spectra of **1** (up) and **1** upon addition of S^{2-} (down) in DMSO-d_6.

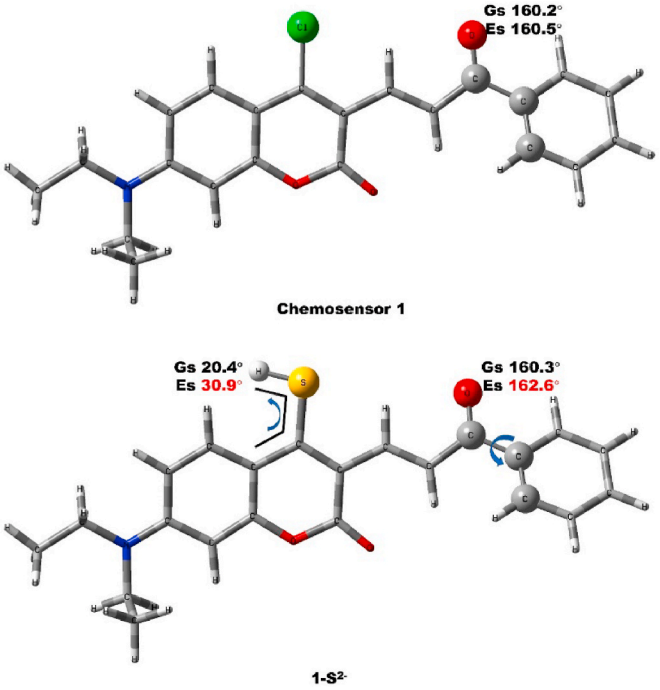

Fig. 5. The optimized geomtry constructions of Chemosensor 1 and 1-S^{2-}. The color coding: blue: nitrogen; red: oxygen; gray: carbon; white: hydrogen; green: chlorine; yellow: sulfur.

In addition to analyze geometries of Chemosensor 1 and 1-S^{2-}, the vertical transition processes of molecules were studied at the molecular level. According to Frank-Condon principle [29,30], a change from one vibrational energy level to another would be more likely to happen if the two vibrational wave functions overlap more significantly upon the photoexcitation process. Herein, the electronic transition probability could be assessed by calculating their oscillator strengths, the oscillator strengths of Chemosensor 1 and 1-S^{2-} jumped from S_0 state to S_1 state were largest, which were 1.4784 and 1.4174 as shown in Table 1. It indicated that the electronic transition occurred mainly in $S_0 \rightarrow S_1$ state. Through the calculation on frontier molecular orbitals (FMOs), we found that electronic transition of two molecules mainly attributed to the highest occupied molecular orbital (HOMO) and the lowest unoccupied molecular orbital (LUMO). The Components index (CI) transition from HOMO to LUMO were 87% and 85% respectively, which indicated that they were the dominant transition processes due to the CI more than 75%. In Fig. 6, we plotted the FMOs isosurfaces of Chemosensor 1 and 1-S^{2-}, the redistribution of electron density mainly occurred in coumarin portion and diethylamine group. Note that a small part of electron density shifted to benzene ring via the bridging effect of ketene group, other small part of electron density shifted from coumarin to halogeno group. From the viewpoint of geometric structures, after the Chemosensor 1 reacted with the analyte, the rotation degrees of benzene ring and sulfydryl group of product 1-S^{2-} increased upon photoexcitation process. This was likely to aggravate molecular twisting charge transfer

Table 1
The major composition of orbital transition with its Components index (CI), and corresponding oscillator strengths for Chemosensor 1 and 1-S^{2-}.

Compounds	Transition	CI	Composition	oscillator strengths
Chemosensor 1	S0→S1	87%	H→L	1.4784
1-S^{2-}	S0→S1	85%	H→L	1.4174

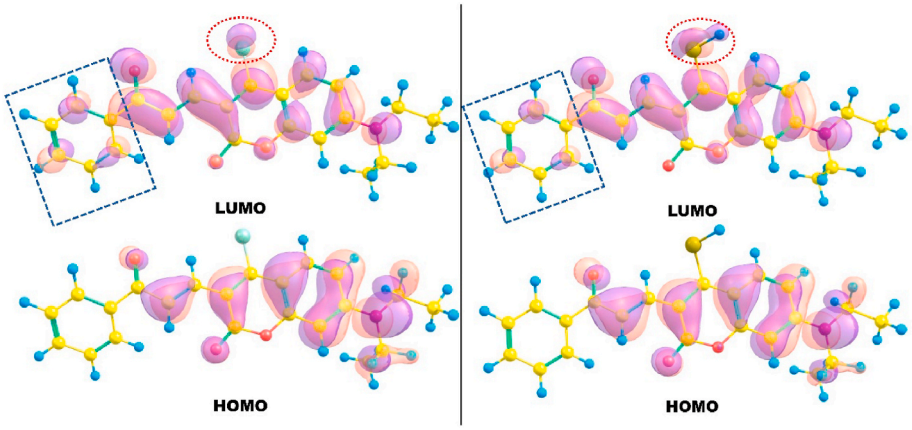

Fig. 6. The visual electron population of the frontier molecular orbitals HOMO and LUMO for Chemosensor 1 and 1-S^{2-}. The blue dotted box represented change of electron density on benzene ring; the red dotted circle represented change of halogeno-groupelectron density.

character, which promoted the fluorescent quenching of 1-S^{2-}.

TDDFT-simulated vertical absorption and emission energies could be used to reproduce the transition spectra in experiment. The theoretical absorption and emission spectra were fitted by Gauss view 5.0 as shown in Fig. 7. The blue and purple dotted lines represented the absorption spectra of Chemosensor 1 and 1-S^{2-}, respectively. The calculated absorption maxima of Chemosensor 1 and 1-S^{2-} were 469 nm and 465 nm respectively, which was agreement with the maxima of 480 nm and 458 nm observed in experiment. In addition to absorption, the emission spectrum of Chemosensor 1 was presented by the red dotted line. The calculated fluorescence peak maximum of Chemosensor 1 was 493 nm, compared with 557 nm observed in experiment, the deviation between the two was less than 0.30 eV. It indicated that the computational method we used was rational to measure the detecting mechanism and its photophysical properties.

Note that the emission spectra of product 1-S^{2-} was not shown in Fig. 7, since the fluorescence of 1-S^{2-} was completely quenched as the concentrations of S^{2-} increased from 0 μmol/L to 10 μmol/L in Fig. 3. Herein, the fluorescent quenching mechanism of 1-S^{2-} was theoretically investigated by constructing the LIICs as shown in Fig. 8. The pathway represented the sulfydryl-group and benzene-ring rotation from Frank-Condon (FC) state to local excited state. It was found that the local excited state structure had an intersystem crossing between the first excited state and second triplet state. According to the analyses of FMOs,

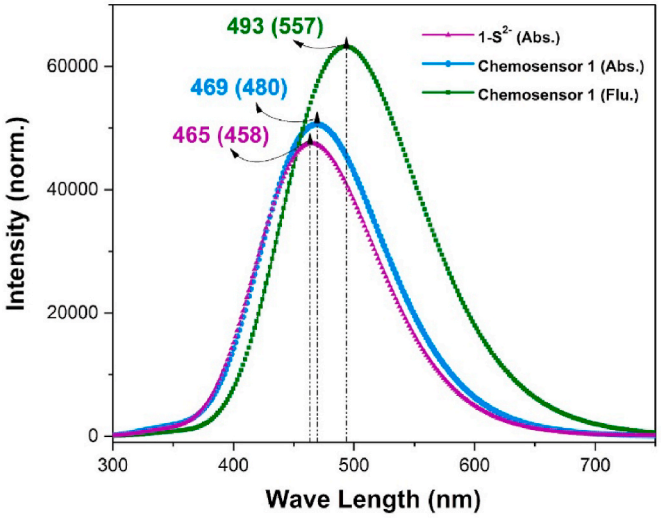

Fig. 7. Theoretical simulating the absorption and emission spectra of the Chemosensor 1 and 1-S^{2-} molecules. The corresponding experiment data was presented in parentheses.

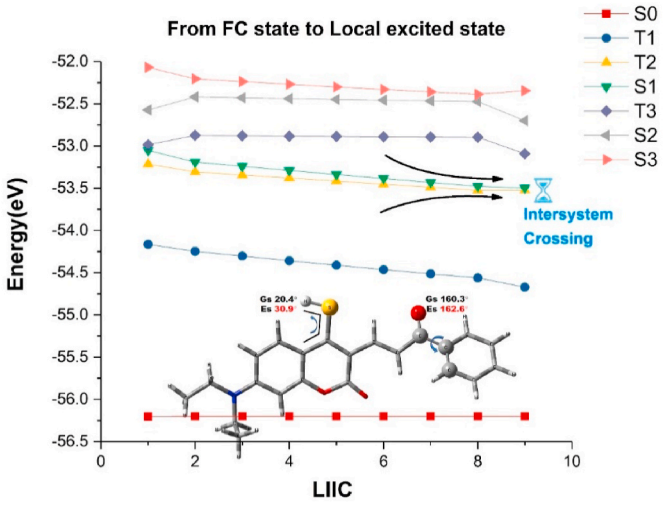

Fig. 8. Constructed minimum energy pathways of different electronic states along linearly interpolated internal coordinates (LIICs) between the Frank-Condon (FC) state and local excited state. The legend represented the different electronic states.

the intersystem crossing accompanied by the slight twisting intramolecular charge transfer in the sulfydryl group and benzene ring, which could be the reason for fluorescent quenching of 1-S^{2-}.

3.6. Analysis of real samples

Chemosensor **1** was also tested for qualitative and quantitative analysis of Na_2S in water samples. For qualitative analysis of sulfur ion in water samples, we designed a visual test paper colorimetric card and inspection process, as shown in Fig. 9. 5 mL of a sample of unknown sulfite concentration was added into the sample bottle, and 2–3 drops of concentrated HCl were added for acidification. The slide containing the prepared wetting test paper was quickly immersed in the sample bottle. After 10 min, the test paper was removed and dried, then moved to a dark box to observe the color change under 365 nm ultraviolet light. Finally, the test results were compared with the colorimetric card to determine whether the environmental samples contained sulfur ions.

For quantitative analysis of sulfite in water samples, we prepared tap water, river water, and sewage samples with added 0.50 μmol/L or 1.50 μmol/L for sulfur ions, as shown in Table 2. The experimental results showed that chemosensor **1** can recognize elevated S^{2-} levels in real samples, and the average of CV and recoveries were satisfactory. This

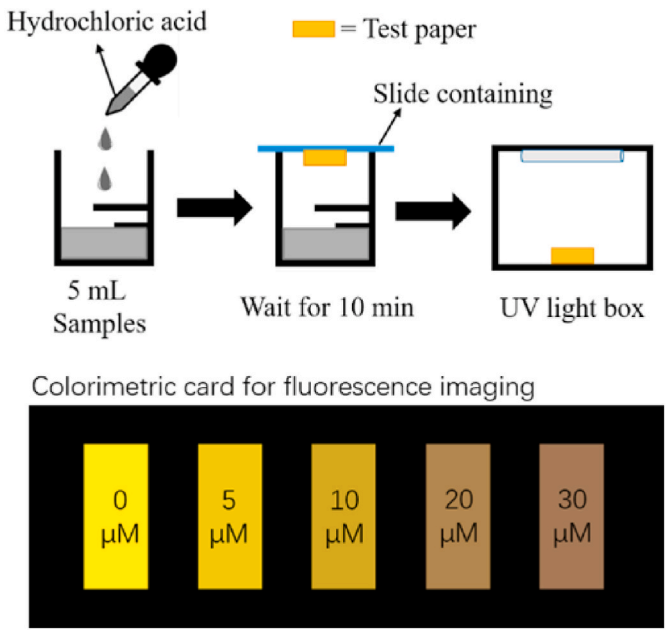

Fig. 9. Flow chart of qualitative analysis of sulfur ion in water samples (up) and colorimetric card for fluorescence imaging (down).

Table 2
Determination of S^{2-} in water samples.

Samples	Na_2S added (μmol/L)	Na_2S found (μmol/L)	CV(%,n = 3)	Recovery (%)
Tap water	–	–	–	–
1	0.50	0.48 ± 0.01	2.1	96.0
2	1.50	1.49 ± 0.01	0.7	99.3
River	0.50	0.47 ± 0.02	4.3	94.0
water	1.50	1.51 ± 0.05	3.3	100.7
1				
2				
Sewage	0.50	0.46 ± 0.03	6.5	92.0
1	1.50	1.47 ± 0.07	4.8	98.0
2				

finding indicates chemosensor **1** has high precision and accuracy for the quantitative detection of S^{2-} in water samples.

4. Conclusions

We have developed a new reaction chemosensor for the detection of S^{2-} based on 4-Cl Coumarin derivatives, and demonstrated the reactive mechanism via fluorescence titration, Job's plot, ESI-MS, ^{1}H NMR, HPLC and Quantum chemistry calculation. The chemosensor displays good selectivity, fast response speed, high sensitivity and easy operation, and results were not impacted by the presence of other analytes. The fluorescence intensity changes of chemosensor **1** (10 μmol/L) in various concentrations of S^{2-} (from 0 μmol/L to 10 μmol/L) showed a linear correlation (R^2 = 0.9997), and the detection limit was calculated as 0.12 μmol/L. In addition, we designed a visual test paper, colorimetric card, inspection process and fluorescence analysis method for the qualitative and quantitative analysis of sulfur ions in water samples.

CRediT authorship contribution statement

Hongda Li: Conceptualization, Formal analysis, Resources, Writing – original draft, Writing – review & editing, Funding acquisition. **Yunfan Yang:** Validation. **Xiaojing Wu:** Visualization. **Rulin Jia:** Investigation. **Pengcheng Zhao:** Project administration. **Yan Wang:** Supervision.

Declaration of competing interest

The authors declare that they have no known competing financial interests or personal relationships that could have appeared to influence the work reported in this paper.

Acknowledgments

This work was supported by the National Natural Science Foundations of China (21804140), Natural Science Foundation of Liaoning Province, China (2020-MS-131), the Technical Research Program of the Ministry of Public Security (2020JSYJC26).

Appendix A. Supplementary data

Supplementary data to this article can be found online at https://doi.org/10.1016/j.dyepig.2021.109373.

References

[1] Huang X, Liu H, Zhang J, Xiao B, Wu F, Zhang Y, et al. A novel near-infrared fluorescent hydrogen sulfide probe for live cell and tissue imaging. New J Chem 2019;43(18):6848–55.
[2] Hammers MD, Taormina MJ, Cerda MM, Montoya LA, Seidenkranz DT, Parthasarathy R, et al. A bright fluorescent probe for H_2S enables analyte-responsive, 3D imaging in live zebrafish using light sheet fluorescence microscopy. J Am Chem Soc 2015;137(32):10216–23.
[3] Sedgwick AC, Wu L, Han H-H, Bull SD, He X-P, James TD, et al. Excited-state intramolecular proton-transfer (ESIPT) based fluorescence sensors and imaging agents. Chem Soc Rev 2018;47(23):8842–80.
[4] Steudel R, Chivers T. The role of polysulfide dianions and radical anions in the chemical, physical and biological sciences, including sulfur-based batteries. Chem Soc Rev 2019;48(12):3279–319.
[5] Hartle MD, Pluth MD. A practical guide to working with H_2S at the interface of chemistry and biology. Chem Soc Rev 2016;45(22):6108–17.
[6] Li H, Zhao P, Zou N, Wang H, Sun K. The colorimetric and ratiometric fluorescent detection of cyanide and sulfide in live cells, application for logic gate and bioimging. Tetrahedron Lett 2017;58(1):30–4.
[7] Lin VS, Chen W, Xian M, Chang CJ. Chemical probes for molecular imaging and detection of hydrogen sulfide and reactive sulfur species in biological systems. Chem Soc Rev 2015;44(14):4596–618.
[8] Luo Y, Zhu C, Du D, Lin Y. A review of optical probes based on nanomaterials for the detection of hydrogen sulfide in biosystems. Anal Chim Acta 2019;1061:1–12.
[9] Tang L, Zhou L, Yan X, Zhong K, Gao X, Liu X, et al. A simple benzothiazole-based mitochondrial-targeting fluorescent probe for visualizing and monitoring viscosity in living cell, lung organ tissue, and living mice. Dyes Pigments 2020;182. 108644.
[10] Tang L, Xia J, Zhong K, Tang Y, Gao X, Li J. A simple AIE-active fluorogen for relay recognition of Cu2+ and pyrophosphate through aggregation-switching strategy. Dyes Pigments 2020;178. 108379.
[11] Li H. A regenerated "turn on" fluorescent probe for sulfide detection in live cells and read samples based on dihydroxyhemicyanine-Cu^{2+} dye. Anal Chim Acta 2018;1010:69–75.
[12] Yang B, Huang J, Bao C, Zhang S, Han Y. A highly sensitive colorimetric and ratiometric fluorescent probe based on 3-hydroxyphthalimide for detection of Hg^{2+} in aqueous solution and its application in real sample analysis. Tetrahedron Lett 2020;61(9). 151534.
[13] Dong J, Hu J, Zhang H. A fast-responsed fluorescent probe for the selective detection hydrogen sulfide and tert- butoxy radical. Tetrahedron 2020;76(28). 131317.
[14] Park S-H, Kwon N, Lee J-H, Yoon J, Shin I. Synthetic ratiometric fluorescent probes for detection of ions. Chem Soc Rev 2020;49(1):143–79.
[15] Li J, Yin C, Huo F. Chromogenic and fluorogenic chemosensors for hydrogen sulfide: review of detection mechanisms since the year 2009. RSC Adv 2015;5(3):2191–206.
[16] Yang M, Fan J, Du J, Peng X. Small-molecule fluorescent probes for imaging gaseous signaling molecules: current progress and future implications. Chem Sci 2020;11(20):5127–41.
[17] Fang Q, Xiong H, Yang L, Wang B, Song X. An instantaneous fluorescent probe for detecting hydrogen sulfide in biological systems. New J Chem 2019;43(34):13594–9.
[18] Liu J, Liu X, Lu S, Zhang L, Feng L, Zhong S, et al. Ratiometric detection and imaging of hydrogen sulfide in mitochondria based on a cyanine/naphthalimide hybrid fluorescent probe. Analyst 2020;145:6549–55.
[19] Zhou N, Yin C, Chao J, Zhang Y, Huo F. An isoxazole-accelerated nitro oxidation type fluorescent detection and imaging for hydrogen sulfide in cells. Sens Actuators, B 2019;287:131–7.
[20] Qian J, Gong D, Teng Z, Wang J, Cao T, Iqbal K, et al. 2-Vinylfuran substituted BODIPY H_2S fluorescent turn on probe based on hydrolysis of furfural and nucleophilic addition of double bond. Sens Actuators, B 2019;297. 126712.

[21] Xie X, Yin C, Yue Y, Chao J, Huo F. Fluorescent probe detect distinguishly sulfite/hydrogen sulfide and thiol via two emission channels in vivo. Sens Actuators, B 2018;277:647–53.
[22] Huang Z, Ding S, Yu D, Huang F, Feng G. Aldehyde group assisted thiolysis of dinitrophenyl ether: a new promising approach for efficient hydrogen sulfide probes. Chem Commun 2014;50(65):9185–7.
[23] Fu L, Tian F-F, Lai L, Liu Y, Harvey PD, Jiang F-L. A ratiometric "two-in-one" fluorescent chemodosimeter for fluoride and hydrogen sulfide. Sens Actuators, B 2014;193:701–7.
[24] Xu C, Li H, Yin B. A colorimetric and ratiometric fluorescent probe for selective detection and cellular imaging of glutathione. Biosens Bioelectron 2015;72:275–81.
[25] Marenich AV, Cramer CJ, Truhlar DG. Universal solvation model based on solute electron density and on a continuum model of the solvent defined by the bulk dielectric constant and atomic surface tensions. J Phys Chem B 2009;113(18):6378–96.
[26] Chai JD, Head-Gordon M. Long-range corrected hybrid density functionals with damped atom-atom dispersion corrections. Physical Chemistry Chemical Physics Pccp 2008;10(44):6615–20.
[27] Tirado-Rives J, Jorgensen WL. Performance of B3LYP density functional methods for a large set of organic molecules. J Chem Theor Comput 2008;4(2):297–306.
[28] Tang B, Yu F, Li P, Tong L, Duan X, Xie T, et al. A near-infrared neutral pH fluorescent probe for monitoring minor pH changes: imaging in living HepG2 and HL-7702 cells. J Am Chem Soc 2009;131(8):3016–23.
[29] Condon E. A theory of intensity distribution in band systems. Phys Rev 1926;28(6):1182–201.
[30] Franck J, Dymond EG. Elementary processes of photochemical reactions. Trans Faraday Soc 1926;21(February):536–42.